EEET ECOLOGICAL ENGINEERING & ENVIRONMENTAL TECHNOLOGY

Ecological Engineering & Environmental Technology, 2026, 27(7), 32–47
https://doi.org/10.12912/27197050/221218
ISSN 2719–7050, License CC-BY 4.0

Received: 2026.04.24
Accepted: 2026.06.15
Published: 2026.07.01

Delineation of subsurface textile waste contamination using electrical resistivity and physicochemical analysis in Bandung, Indonesia

Muhammad Syukri[1,2*], Eleonora Agustine[3], Haris Saputra[4], Rini Safitri[1], Anis Surita Ilda[2], Putri Navila Agustina[2]

[1] Department of Physics, Faculty of Mathematics and Natural Sciences, Universitas Syiah Kuala, Banda Aceh, 23111, Indonesia
[2] Department of Geophysics Engineering, Faculty of Engineering, Universitas Syiah Kuala, Banda Aceh, 23111, Indonesia
[3] Department of Geophysics, Faculty of Mathematics and Natural Sciences, Universitas Padjadjaran, Sumedang, 45363, Indonesia
[4] Department of Civil Engineering, Faculty of Engineering, Universitas Muhammadiyah Aceh, Banda Aceh, 23123, Indonesia
* Corresponding author's e-mail: m.syukri@usk.ac.id

ABSTRACT

Industrial wastewater discharge from textile industries poses a significant threat to subsurface environmental quality, particularly in complex geological settings where contaminant migration is difficult to detect using surface observations alone. This study aims to delineate and characterize subsurface contamination associated with textile industrial waste in the Cikijing River, Bandung, Indonesia, with particular emphasis on its occurrence within a volcanic–structural geological environment. An integrated approach was employed by combining electrical resistivity tomography (ERT) and physicochemical analyses. ERT surveys using a dipole–dipole configuration were conducted along four profiles, while sediment samples were analyzed for pH, electrical conductivity (EC), and total dissolved solids (TDS) to validate geophysical interpretations. The inversion results reveal a stratified subsurface consisting of topsoil, clay, and dense sandy gravel layers. A prominent low-resistivity anomaly ranging from 2.63 to 9.82 Ωm was identified within the clay layer at depths of 0.5 to 4.3 m, extending laterally up to 22.5 m. This anomaly is interpreted as a contaminant plume resulting from the accumulation and retention of industrial effluents within low-permeability materials. Physicochemical measurements support this interpretation, showing acidic conditions (pH 5.4–5.7), elevated EC values reaching 2,710 µS/cm, and high TDS concentrations exceeding 1,999 ppm, all of which surpass WHO and national environmental standards. These findings confirm the significant impact of textile wastewater infiltration on subsurface conditions. Nevertheless, the results provide practical value for environmental assessment, pollution monitoring, and remediation planning in industrial regions. The originality of this research lies in integrating geophysical and physicochemical approaches to delineate contamination within a volcanically influenced and structurally controlled subsurface system, offering new insights into contaminant behavior in complex geological environments.

Keywords: textile wastewater, electrical resistivity tomography, subsurface contamination, physicochemical analysis, Cikijing river.

INTRODUCTION

The rapid expansion of industrial activities, particularly in the textile sector, has become a major driver of environmental degradation, especially in river ecosystems. Textile industries are known to produce large volumes of wastewater containing dyes, heavy metals, and complex organic compounds, all of which can significantly alter the physicochemical characteristics of water

and soil (Zhou et al., 2022; Ahsan et al., 2019; Kanan et al., 2014). When this wastewater is discharged without proper treatment, pollutants can accumulate in surface water and gradually infiltrate into subsurface layers, thereby posing long-term risks to groundwater systems and overall ecological sustainability (Zhou et al., 2022; Angi et al., 2025). In many developing regions, this situation is further complicated by weak enforcement of environmental regulations, allowing contamination to persist and intensify over time.

The Cikijing River in Bandung Regency, Indonesia, represents a clear example of this issue. Flowing through the Rancaekek industrial area, which is dominated by textile factories, the river has been subjected to continuous exposure to industrial discharge. Previous studies have documented elevated concentrations of heavy metals such as Pb, Cd, and Cr in both water and sediment, underscoring the severity of contamination and its associated ecological risks (Marselina and Wijaya, 2024; Novaliana et al., 2025). Other investigations have also detected pollution signals using geophysical and magnetic approaches within the same river system (Prananda et al., 2017). Despite these findings, most existing studies are still limited to surface observations and do not adequately capture subsurface contamination processes.

Water quality is commonly evaluated using physicochemical parameters such as pH, EC, and TDS, which provide essential information on acidity, ionic content, and the overall concentration of dissolved materials (Bakar et al., 2020; Maleck et al., 2024; Adestina et al., 2024). While these parameters are useful, they are typically measured at discrete sampling points, thereby limiting their ability to represent spatial variability and subsurface contaminant transport pathways. This limitation is particularly significant in textile-impacted environments, where contaminants can migrate beyond the river channel and spread into shallow groundwater systems (Zhou et al., 2022).

To overcome these limitations, geophysical methods – especially electrical resistivity tomography (ERT) – have increasingly been used in environmental studies. ERT offers a non-invasive technique to image subsurface conditions by measuring variations in electrical resistivity, which are influenced by factors such as lithology, porosity, moisture content, and ionic concentration (Bernardo et al., 2022; Kondracka et al., 2021). In contaminated environments, resistivity values tend to decrease due to the presence of conductive fluids enriched with dissolved ions (Ibuot et al., 2017; Syukri et al., 2013). A number of studies have successfully applied ERT to detect contamination in waste disposal sites, including landfills and open dumping areas (Appiah et al., 2018; Boonsakul et al., 2023; Suknark et al., 2023). Moreover, combining geophysical methods with physicochemical analysis has been shown to improve the reliability of environmental assessments by linking subsurface anomalies with quantitative pollutant indicators (Ibuot et al., 2024).

In the Indonesian context, geoelectrical methods have been applied in various environmental and geotechnical studies, including contamination mapping and subsurface characterization (Ashel et al., 2021; Syukri et al., 2020). In the Linggar area and its surroundings, previous work has identified contamination using resistivity data; however, these studies often suffer from limited spatial coverage or lack robust integration with detailed physicochemical measurements, resulting in incomplete interpretation of contamination processes.

From a hydrogeological standpoint, the movement of contaminants is strongly influenced by subsurface conditions such as lithology, permeability, and groundwater flow patterns. The Bandung Basin is dominated by alluvial deposits composed of clay, silt, and sand, which can facilitate contaminant transport, particularly in more permeable layers. Under such conditions, pollutants can spread both laterally along the river and vertically into deeper subsurface zones, thereby increasing the vulnerability of groundwater resources (Silitonga, 1973).

Despite the progress made in environmental geophysics, several important gaps remain. Many previous studies tend to rely on either physicochemical analysis or geophysical methods alone, without fully integrating both approaches in a quantitative framework. In addition, studies conducted in the Cikijing River area have not clearly established a quantitative relationship between resistivity anomalies and key water quality parameters such as EC and TDS. Research focusing specifically on textile-related contamination in river systems is also still limited, as most existing work has concentrated on landfill or mining environments. Furthermore, there is still a lack of studies that explicitly link geophysical observations with hydrogeological processes to explain contaminant migration in subsurface environments.

To address this gap, this study aims to identify and characterize subsurface electrical anomalies

potentially associated with textile industrial effluents in the Cikijing River area by integrating ERT with physicochemical parameters (pH, EC, and TDS), in order to improve the interpretation of contamination processes in heterogeneous alluvial environments.

The study is guided by the following scientific hypotheses. H1 (geophysical response hypothesis): low-resistivity anomalies in the shallow subsurface are associated with zones of increased pore-water conductivity potentially influenced by anthropogenic inputs. H2 (hydrochemical consistency hypothesis): zones characterized by low resistivity are associated with sediments exhibiting elevated EC and TDS values and altered pH conditions. H3 (hydrogeological control hypothesis): the distribution and continuity of subsurface anomalies are influenced by lithological structure, with clay-rich layers potentially acting as pathways and/or reservoirs for contaminant accumulation. H4 (methodological hypothesis): the integration of ERT and physicochemical analysis provides a more consistent and reliable interpretation of subsurface conditions compared to the use of a single method alone.

The significance of this study lies in its ability to bridge methodological and practical gaps. By combining geophysical imaging with laboratory-based analysis, it offers a robust framework for identifying and validating contamination zones. Ultimately, these findings provide new insights into how textile-derived pollutants migrate within riverine subsurface environments, supporting more effective environmental monitoring and sustainable management strategies in Indonesia.

GENERAL GEOLOGY OF STUDY AREA

The study area is located in the Rancaekek District, eastern Bandung Basin, Indonesia. The Bandung Basin is an intermontane basin formed during the Quaternary as a result of volcanic activity and tectonic deformation. It is widely interpreted as a former lacustrine system that was progressively infilled by volcanic and sedimentary deposits, resulting in a heterogeneous subsurface structure (Silitonga, 1973; Sabrian et al., 2024; Satriyo et al., 2025).

According to regional geological mapping, the study area is dominated by the Lake Deposits Formation (Ql) (Figure 1), which consists primarily of tuffaceous clay, tuffaceous sandstone, and tuffaceous gravel (Silitonga, 1973). These lithologies indicate deposition in a low-energy lacustrine environment with significant volcanic input. Locally, the formation contains calcareous concretions, plant remains, freshwater mollusks, and vertebrate fossils, reflecting mixed volcanic, sedimentary, and biological influences on deposition.

At the basin scale, subsurface materials comprise unconsolidated to semi-consolidated Quaternary deposits, including lacustrine sediments, alluvial deposits, and volcanic products. This lithological variability produces strong spatial heterogeneity in porosity and permeability, which directly controls groundwater flow and contaminant transport (Satriyo et al., 2025).

Hydrogeologically, the subsurface is characterized by interbedded fine-grained units (clay and silt) and coarser permeable units (sand and gravel), forming a multilayered aquifer system. Permeable layers facilitate groundwater flow and act as preferential pathways for contaminant migration, whereas fine-grained layers function as semi-confining units that retard vertical flow and promote the accumulation of contaminants. These contrasts are critical for geoelectrical interpretation, as resistivity values are strongly influenced by lithology, pore structure, and fluid conductivity. Clay-rich and saturated zones containing dissolved ions typically exhibit low resistivity, whereas coarser and less saturated materials tend to show higher resistivity responses.

Structural features also influence groundwater flow within the basin. Fault systems, including the Lembang Fault, may act either as conduits or barriers depending on their hydraulic properties (Delinom, 2009). In this study, the relative position of the study area with respect to major fault structures is considered in interpreting subsurface flow patterns and possible preferential migration pathways, although detailed structural measurements are beyond the scope of this work.

Groundwater conditions in the Bandung Basin have been significantly affected by anthropogenic activities, particularly industrial development and groundwater extraction. Reported impacts include declining groundwater levels, reduced water quality, and increased susceptibility to contamination (Wangsaatmaja et al., 2006; Tirtomihardjo, 2016). Land subsidence associated with long-term groundwater withdrawal has also been documented and may alter subsurface hydraulic properties and flow patterns (Maryudhaningrum et al., 2025).

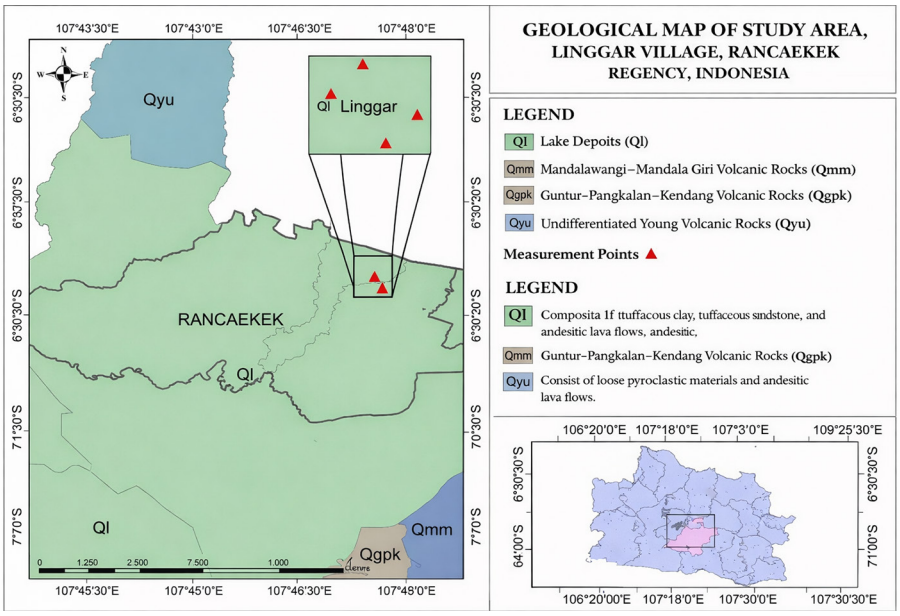

Figure 1. Regional geological map of the Bandung Quadrangle (modified Silitonga, 1973)

In the Rancaekek area, shallow groundwater conditions combined with permeable sediment layers enhance the potential for both lateral and vertical contaminant migration. These hydrogeological conditions directly influence the distribution of conductive fluids in the subsurface, which is reflected in resistivity variations obtained from ERT measurements.. Overall, the geological and hydrogeological setting – characterized by lacustrine deposits, volcanic influence, layered aquifer systems, and anthropogenic stress – provides a controlling framework for fluid movement and contaminant transport. This framework is essential for interpreting resistivity anomalies and delineating contamination zones in the subsurface.

MATERIALS AND METHODS

Study area and data acquisition

Geoelectrical measurements and sediment sampling were conducted in the vicinity of the Cikijing River, Bandung Regency, Indonesia. The survey area was selected based on its proximity to textile industrial activities and documented evidence of surface water degradation, indicating a high likelihood of contaminant infiltration into the subsurface system.

A total of four geoelectrical survey lines (Lines 1–4) were established (Figure 2). The geographic coordinates and elevations of each line are provided in Table 1. All coordinates were recorded using the WGS84 datum. Each survey line had a length of 24 m with an electrode spacing of 0.5 m, resulting in a total of 48 electrodes per line. The orientation (azimuth) of the lines ranged between 80° and 110°, designed to be both perpendicular and sub-parallel to the river flow in order to capture lateral and longitudinal variations in subsurface conditions. The spacing between adjacent lines ranged from 5 to 10 m. The topography along the survey lines is relatively flat, with elevation differences less than 2 m, and therefore no topographic correction was applied during inversion.

Sediment samples were collected from Lines 3 and 4, which are located closest to the riverbank (approximately 1–3 m) and aligned sub-parallel to the river flow. These locations were selected based on field evidence, including visible wastewater discharge points, discoloration of river water, and accumulation of fine-grained sediments, indicating enhanced contaminant deposition.

Geoelectrical data processing was performed at the Geophysics Laboratory, Universitas Syiah Kuala. Physicochemical analysis (pH, EC, and TDS) was conducted at the Geophysics Laboratory, Universitas Padjadjaran.

Samples were stored in sealed polyethylene bags immediately after collection, transported within 24 hours, and analyzed within 48 hours. Samples were air-dried prior to analysis to ensure measurement consistency.

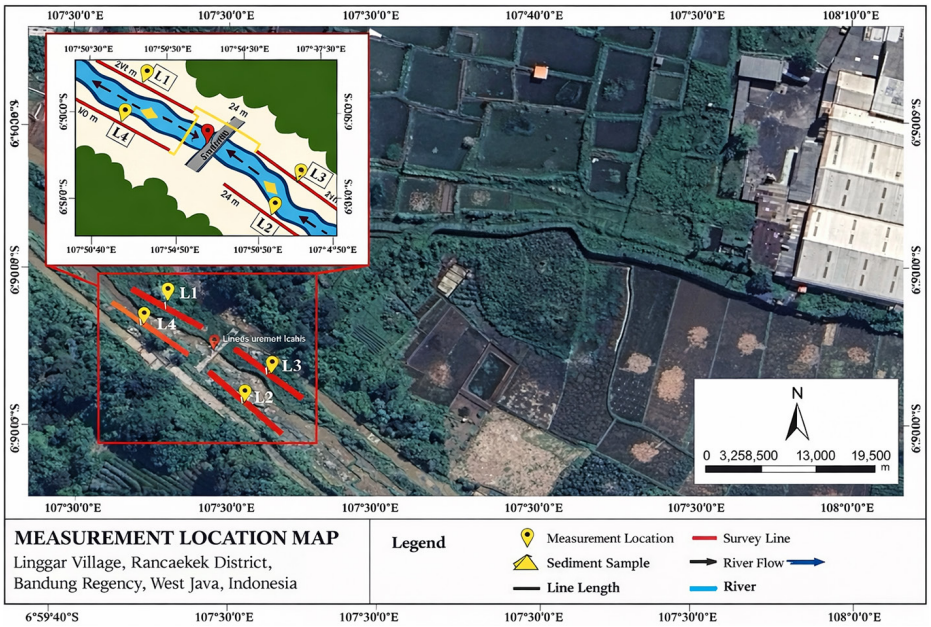

Figure 2. Schematic map showing the layout of survey lines in the study area

Table 1. Coordinates and elevation of survey lines

No	Survey line	Coordinates	Elevation (m)
1	Line 1	6°58'2.00"S; 107°47'33.01"E	674
2	Line 2	6°58'2.81"S; 107°47'33.89"E	686
3	Line 3	6°58'3.04"S; 107°47'33.69"E	690
4	Line 4	6°58'2.26"S; 107°47'32.68"E	679

Electrical resistivity survey

The geoelectrical survey was conducted using a dipole–dipole configuration, which employs two current electrodes and two potential electrodes to inject and measure electrical current within the subsurface. In this configuration, the spacing between adjacent electrodes is defined as a, while the separation between the current and potential electrode pairs is expressed as na, where n represents the level of investigation depth (Syukri et al., 2025a). This arrangement allows for enhanced sensitivity to lateral resistivity variations, making it suitable for identifying contamination zones.

The dipole–dipole configuration was selected due to its high lateral resolution and effectiveness in resolving shallow subsurface heterogeneity, which is particularly important in environmental studies where contaminant distribution is spatially variable and controlled by near-surface processes.

The apparent resistivity values were calculated using a geometric factor (K), which accounts for the spatial arrangement of the electrodes. For the dipole–dipole configuration, the geometric factor can be expressed as:

$$K = \pi an(n+1)(n+2) \quad (1)$$

where: K is the geometric factor, a is the electrode spacing, and n is the level number corresponding to the depth of investigation (Alao et al., 2024; De Borba et al., 2023).

The maximum dipole separation level used was n = 6, resulting in an approximate depth of investigation of 4–5 m. No roll-along technique was applied, as each survey line length was fixed at 24 m. The dipole–dipole array was selected due to its high sensitivity to lateral resistivity variations and suitability for imaging shallow heterogeneous environments.

Data acquisition

The geoelectrical survey was conducted using an RMSS Marcapada resistivity meter along four survey lines, each extending 24 m with an electrode spacing of 0.5 m. During data acquisition, field conditions along each line were systematically observed and documented, and the coordinates of each survey line were recorded. Prior to measurement, a stable working area was prepared, and a measuring tape was laid out along the predefined survey lines.

Electrodes were installed at regular intervals of 0.5 m and connected using electrode cables. The instrument was powered and connected to the electrode system, followed by the configuration of measurement parameters, including electrode arrangement, number of electrodes, and spacing (Figure 3). A resistance check was performed to ensure optimal electrode-ground contact before initiating data acquisition. Once the system was ready, measurements were carried out, and the acquired data were automatically stored in the device's internal memory for further processing.

Contact resistance was measured prior to acquisition and maintained below 2 kΩ. Electrodes exceeding this threshold were reinstalled or the soil was conditioned to improve contact. Each measurement point was recorded using a stacking factor of 3–5 cycles to improve signal quality. Data acquisition was conducted under dry weather conditions with relatively stable soil moisture. Measurements were performed during daytime (09:00–15:00) to ensure consistent environmental conditions. Repeated measurements were performed at selected points to verify data consistency, and unstable or noisy readings were re-measured or removed during processing.

Data processing

The acquired data were initially stored in.dat format. These data were then organized using Microsoft Excel by extracting key parameters such as datum, electrode spacing, n-factor, and apparent resistivity (Figure 4). The processed data were subsequently saved in.txt format for inversion. Data inversion was carried out using RES2DINV software, applying a least-squares inversion method to generate two-dimensional resistivity models (Figure 5). These models were used to represent the spatial distribution of subsurface resistivity (Eze et al., 2022; Loke, 2004).

A smoothness-constrained least-squares (L2-norm) inversion scheme was applied. The inversion process was iterated 4–6 times until the root mean square (RMS) error was reduced below 25% or showed no significant improvement. Default regularization parameters were used. Outlier data points were removed prior to inversion based on abnormal resistivity values and inconsistent measurements. No topographic correction was applied due to minimal elevation variation.

Data interpretation

Resistivity values measured in the field are influenced by several subsurface properties, including lithology, porosity, water content, and ionic concentration. In general, materials with high water content and dissolved ions tend to exhibit lower resistivity values, while dry or compact materials show higher resistivity (Syukri et al., 2025b; Lowrie and Fichtner, 2020).

In the context of environmental contamination, zones affected by industrial wastewater typically display lower resistivity due to the presence of conductive fluids enriched with dissolved ions. The interpretation of resistivity data in this study was therefore guided by standard resistivity ranges for geological materials (Saputra et al.,

Figure 3. Data acquisition procedure using the RMSS Marcapada resistivity meter

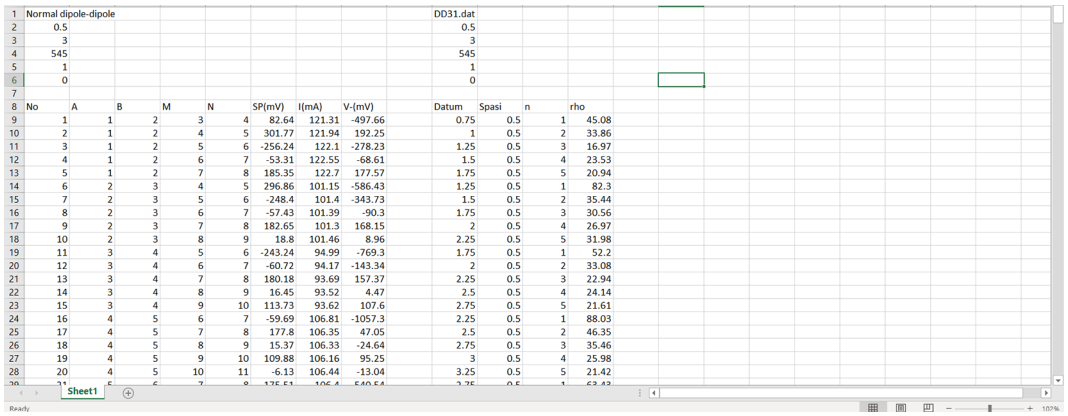

1	Normal dipole-dipole								DD31.dat				
2	0.5								0.5				
3	3								3				
4	545								545				
5	1								1				
6	0								0				
7													
8	No	A	B	M	N	SP(mV)	I(mA)	V-(mV)	Datum	Spasi	n	rho	
9	1	1	2	3	4	82.64	121.31	-497.66	0.75	0.5	1	45.08	
10	2	1	2	4	5	301.77	121.94	192.25	1	0.5	2	33.86	
11	3	1	2	5	6	-256.24	122.1	-278.23	1.25	0.5	3	16.97	
12	4	1	2	6	7	-53.31	122.55	-68.61	1.5	0.5	4	23.53	
13	5	1	2	7	8	185.35	122.7	177.57	1.75	0.5	5	20.94	
14	6	2	3	4	5	296.86	101.15	-586.43	1.25	0.5	1	82.3	
15	7	2	3	5	6	-248.4	101.4	-343.73	1.5	0.5	2	35.44	
16	8	2	3	6	7	-57.43	101.39	-90.3	1.75	0.5	3	30.56	
17	9	2	3	7	8	182.65	101.3	168.15	2	0.5	4	26.97	
18	10	2	3	8	9	18.8	101.46	8.96	2.25	0.5	5	31.98	
19	11	3	4	5	6	-243.24	94.99	-769.3	1.75	0.5	1	52.2	
20	12	3	4	6	7	-60.72	94.17	-143.34	2	0.5	2	33.08	
21	13	3	4	7	8	180.18	93.69	157.37	2.25	0.5	3	22.94	
22	14	3	4	8	9	16.45	93.52	4.47	2.5	0.5	4	24.14	
23	15	3	4	9	10	113.73	93.62	107.6	2.75	0.5	5	21.61	
24	16	4	5	6	7	-59.69	106.81	-1057.3	2.25	0.5	1	88.03	
25	17	4	5	7	8	177.8	106.35	47.05	2.5	0.5	2	46.35	
26	18	4	5	8	9	15.37	106.33	-24.64	2.75	0.5	3	35.46	
27	19	4	5	9	10	109.88	106.16	95.25	3	0.5	4	25.98	
28	20	4	5	10	11	-6.13	106.44	-13.04	3.25	0.5	5	21.42	

Figure 4. Data processing workflow in Microsoft Excel showing the extraction of datum, electrode spacing, n-factor, and apparent resistivity parameters

2024; Reynolds, 2011), enabling the delineation of lithological units and identification of potential contamination zones.

However, it is important to note that low resistivity values may also be associated with clay-rich lithologies or high natural moisture content. Therefore, resistivity anomalies alone are not considered definitive indicators of contamination without supporting physicochemical data.

Laboratory analysis

Sediment sampling

Sediment samples were collected from Lines 3 and 4 to support geophysical interpretation through physicochemical analysis. These locations were selected based on their proximity to the river flow and their high likelihood of contaminant accumulation. Each sample was stored in a sealed plastic bag to maintain its condition during transport.

Sample preparation

The collected samples were first dried to remove moisture content and ensure measurement consistency. During drying, samples were covered to prevent contamination from the surrounding environment. After drying, the samples were crushed and sieved using a 120-mesh sieve to obtain a homogeneous and representative material suitable for analysis (Figure 6).

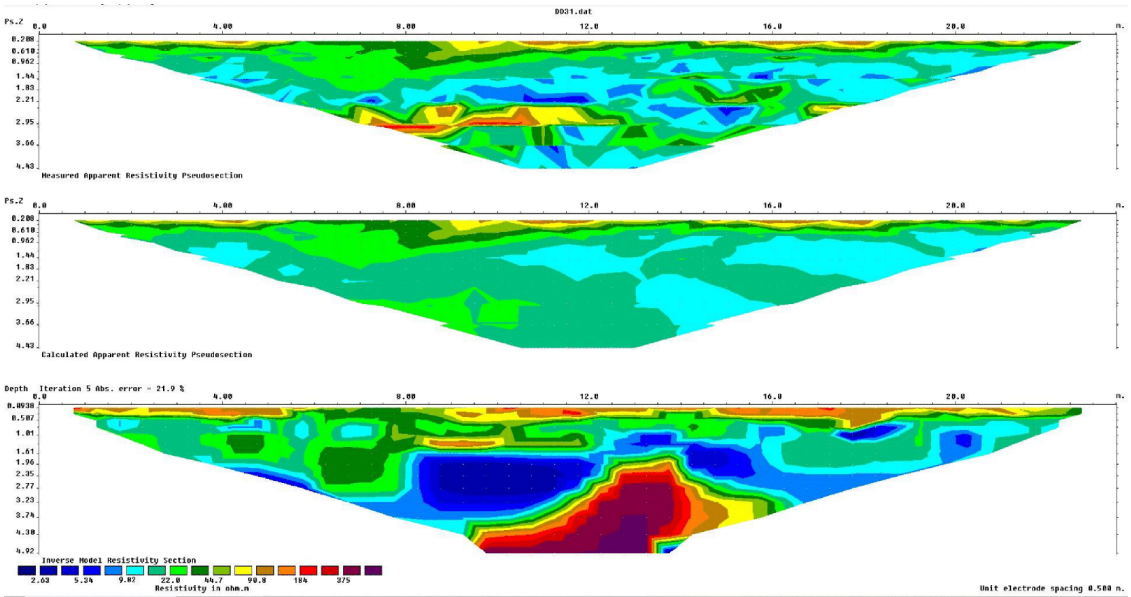

Figure 5. Two-dimensional resistivity model generated through least-squares inversion using RES2DINV software

(a) (b)

Figure 6. Laboratory preparation of sediment samples: (a) sieving using a 120-mesh sieve and b) drying process prior to analysis

Laboratory measurement

Physicochemical parameters, including pH, EC, and TDS, were measured using a Hanna Combo Meter HI9813-6 (Figure 7). Each sediment sample was mixed with distilled water at a ratio of 1:2.5 (w/v), homogenized, and allowed to stabilize for 10–15 minutes at room temperature (~25 °C). To ensure reproducibility and analytical reliability, each parameter was measured in triplicate. The instrument was rinsed with distilled water between measurements to prevent cross-contamination.

Data interpretation

To support the geophysical interpretation, physicochemical analysis was conducted using three key parameters: EC, pH, and TDS. These parameters provide important information about water quality and are commonly used as indicators of contamination.

EC reflects the ability of water to conduct electrical current, which is directly related to the concentration of dissolved ions. Higher EC values generally indicate elevated ionic content and deteriorated water quality (Nugroho et al., 2025).

The pH value represents the acidity or alkalinity of water and typically ranges from 1 to 14. Neutral water conditions fall within the range of 6.5–8.5, while values outside this range may indicate contamination or chemical imbalance (Geetha et al., 2024). Variations in pH can be influenced by factors such as dissolved gases, carbonate content, and organic decomposition.

TDS represent the total concentration of dissolved substances in water, including inorganic salts and organic matter. High TDS levels may indicate environmental pollution and can negatively affect aquatic ecosystems. According to established standards, TDS values exceeding 1000 mg/L are considered unsuitable for aquatic life and may pose environmental risks (Rifai and Harintaka, 2025).

RESULTS AND DISCUSSION

Geoelectrical data processing results

The geoelectrical data processing was conducted through a series of systematic steps to convert raw field measurements into reliable subsurface models. Initially, field data were organized and prepared to ensure compatibility with the processing software. The dataset was then imported into RES2DINV to generate the measured apparent resistivity pseudosection as the initial representation of subsurface conditions (Figure 5). Subsequently, forward modeling was performed to obtain the calculated apparent resistivity pseudosection for comparison with the field data. An iterative inversion process using a least-squares approach was applied to minimize the difference between measured and calculated values, as indicated by the RMS error. The final output is the inverse model resistivity section, which represents the subsurface resistivity distribution and forms the primary basis for geological and contamination interpretation across all survey lines.

Based on the processing results using RES2DINV, all four survey lines show a maximum investigation depth of approximately 4.9 m, with resistivity values ranging from 2.63 Ωm to 375 Ωm. Each line produces three types of 2D pseudosections, as presented in Figures 8 to 11. The measured apparent resistivity pseudosection

(a) (b)

Figure 7. Measurement of physicochemical parameters (pH, EC, and TDS): (a) sample measurement procedure and (b) Hanna Combometer HI9813-6 used in the analysis

represents the raw field data prior to inversion, generally showing a dominant resistivity range of 9.82–22 Ωm, with wider variations observed in certain survey lines. The calculated apparent resistivity pseudosection, generated through forward modeling, presents a more constrained range of 9.82–98.8 Ωm and reflects the modeled response of the subsurface. Finally, the inverse model resistivity section provides the most representative subsurface condition, with values ranging from low resistivity (2.63–9.82 Ωm), typically associated with highly conductive zones, to moderate resistivity (22.0–44.7 Ωm). These general patterns indicate consistent subsurface behavior with localized anomalies interpreted as contamination zones, which are further discussed in detail below.

Subsurface interpretation – Line 1

Based on the 2D inversion section shown in Figure 8, three main subsurface layers can be identified along Line 1. The shallow layer at a depth of 0–0.5 m, extending from 0.75 m to 22.75 m along the profile, exhibits resistivity values ranging from 106 Ωm to 174 Ωm and is interpreted as topsoil. This layer shows no indication of contamination, suggesting relatively stable near-surface conditions consistent with field observations.

Beneath this, a clay layer dominates from 0.5 m to 4.9 m depth with resistivity values between 22.0 Ωm and 98.8 Ωm. Within this unit, a distinct low-resistivity anomaly (2.63–9.82 Ωm) is observed between depths of 0.5 m and 4.2 m, extending laterally from approximately 1.5 m to 22 m. This anomaly is interpreted as a contaminated clay layer, indicating the accumulation and lateral spreading of conductive contaminants derived from industrial wastewater infiltration.

At greater depths, a high-resistivity zone ranging from 184 Ωm to 376 Ωm appears At greater depths, a high-resistivity zone ranging from 184 Ωm to 376 Ωm appears between 1.9 m and 4.9 m depth, particularly between 9.5 m and 14.5 m along the line. This zone is interpreted as compact sandy gravel. The absence of low-resistivity anomalies in this layer suggests that contamination has not penetrated this unit, likely due to reduced porosity and limited hydraulic connectivity.

Subsurface interpretation – Line 2

Based on the 2D inversion results shown in Figure 9, three distinct subsurface layers are identified: topsoil, clay, and compact dry sandy gravel. The dominant feature is the clay layer, located at depths ranging from 0.5 m to 4.5 m. Within this unit, a significant low-resistivity anomaly is observed between depths of 0.5 m and 4.3 m, extending laterally from 1.25 m to 22.25 m.

This zone is interpreted as contaminated clay, demonstrating a continuous lateral plume consistent with infiltration-driven contaminant transport. The contamination pattern is particularly pronounced at shallow depths (0.5–1.5 m), indicating active near-surface infiltration processes.

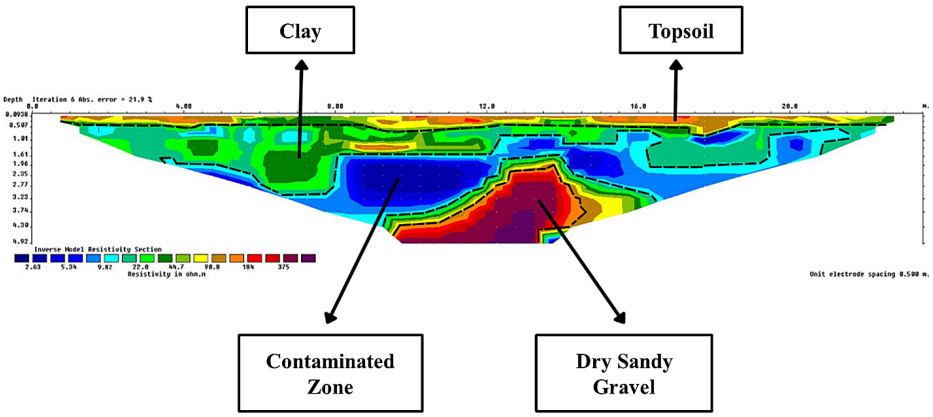

Figure 8. 2D inverse resistivity section of Line 1 illustrating the lateral and vertical variation of subsurface materials, with low-resistivity zones indicating potential contamination and higher resistivity zones representing more compact formations

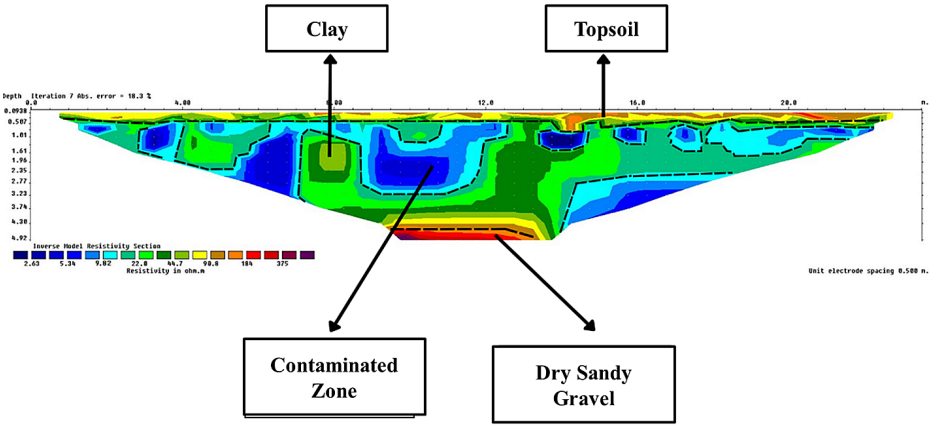

Figure 9. 2D inverse resistivity section of Line 2 illustrating the lateral and vertical variation of subsurface materials, with low-resistivity zones indicating potential contamination and higher resistivity zones representing more compact formations

The topsoil layer (0–0.5 m) and compact sandy gravel at greater depths do not exhibit contamination signatures, suggesting that contaminant migration remains largely confined within the clay unit, similar to the pattern observed in Line 1.

Subsurface interpretation – Line 3

Based on the 2D inversion section shown in Figure 10, the subsurface consists of topsoil, clay, and compact sandy gravel. Within the clay unit, a low-resistivity anomaly is observed between depths of 0.5 m and 3.3 m, extending laterally from 1.25 m to 22.5 m.

Compared to Lines 1 and 2, the contamination pattern in Line 3 appears more concentrated. This intensification is likely associated with localized hydrodynamic conditions and proximity to direct industrial discharge sources, which enhance contaminant accumulation. The interaction between river flow and the survey line orientation likely promotes focused infiltration and higher contaminant loading, resulting in a denser anomaly signature.

Subsurface interpretation – Line 4

Figure 11 shows the 2D resistivity profile for Line 4. Similar to other lines, three main layers are identified: topsoil, clay, and compact sandy gravel. A prominent low-resistivity anomaly is observed within the clay layer between depths of 0.5 m and 3.8 m, extending laterally from 1.25 m to 22 m.

This anomaly is interpreted as a contaminant plume, indicating persistent subsurface pollution consistent across all survey lines. The repetition of this pattern strengthens the interpretation that

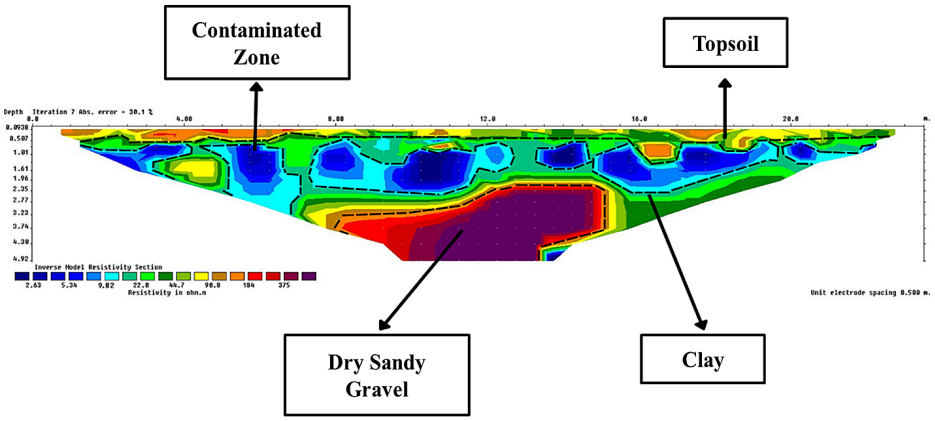

Figure 10. 2D inverse resistivity section of Line 3 illustrating the lateral and vertical variation of subsurface materials, with low-resistivity zones indicating potential contamination and higher resistivity zones representing more compact formations

contamination is not localized but regionally distributed within the study area.

Subsurface characterization and contaminant distribution

Based on the resistivity ranges established by Syukri et al. (2013), Reynolds (2011), and Telford et al. (1990), the subsurface materials are primarily associated with clay and dense sandy gravel. This interpretation is corroborated by Dewi et al. (2020), who identified similar lithological characteristics in the Bandung Basin.

The zones impacted by industrial waste are clearly delineated by significantly low resistivity values (2.63–9.82 Ωm), indicating high ionic concentration and enhanced electrical conductivity. These findings are consistent with Miswar (2017) and Fitriani et al. (2021), confirming the presence of heavy metal contamination.

A consistent low-resistivity anomaly observed across all lines suggests the presence of a continuous contaminant plume system, likely facilitated by the hydrogeological properties of the clay layer. Although clay typically acts as a barrier, its partial permeability and fissuring can enable slow but persistent contaminant migration (Ashel et al., 2021).

This study highlights a key scientific finding: the clay layer does not function solely as an impermeable barrier but also acts as both a contaminant storage medium and a preferential lateral transport pathway, as evidenced by the repeated anomaly distribution across all profiles.

The inversion results (Table 2) indicate that the clay layer serves as the primary zone for contaminant accumulation and lateral transport, functioning as both a storage medium and a migration pathway for industrial effluents.

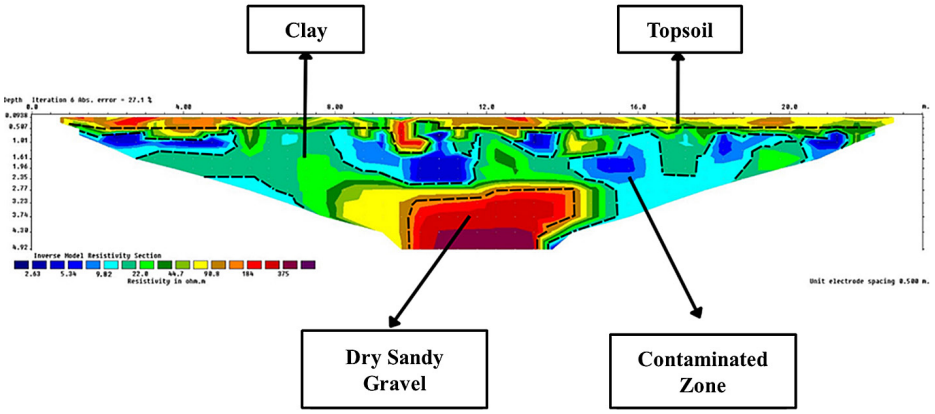

Figure 11. 2D inverse resistivity section of Line 4 illustrating the lateral and vertical variation of subsurface materials, with low-resistivity zones indicating potential contamination and higher resistivity zones representing more compact formations

Physicochemical analysis

To substantiate the resistivity anomalies observed in the geophysical profiles, the physicochemical properties of the Cikijing River sediments were evaluated. Sediment samples were strategically collected from two distinct locations: point sdm1, representing the upstream sector, and point sdm2, situated in the downstream reach. The analysis focused on three critical environmental indicators – pH, EC, and TDS – to determine the extent of industrial impact on the riverine system. The analytical results for both sampling stations are summarized in Table 3.

pH Level analysis

According to established environmental quality standards, non-polluted freshwater typically maintains a pH range between 6.5 and 8.5 (Kirana et al., 2026). However, the physicochemical results presented in Table 3. demonstrate that both sdm1 and sdm2 fall significantly outside the permissible limits set by the Ministry of Health of the Republic of Indonesia. The recorded pH values at these sampling points were 5.4 and 5.7, respectively, categorizing the river water as acidic.

This acidification is likely attributed to elevated concentrations of dissolved heavy metals within the study area (Putri and Afdal, 2023). The presence of acidic conditions often enhances the solubility and mobility of metallic ions, further exacerbating the toxicological risk to the riverine environment. Consequently, based on the observed pH levels, the Cikijing River exhibits clear characteristics of severe contamination, rendering the aquatic environment hazardous for the survival of local biota and detrimental to the overall health of the ecosystem.

The analytical results presented in Table 3. reveal that the highest EC occurs at station sdm1 (upstream), reaching an average value of 2.710 µS/cm. This elevated conductivity is likely attributed to the proximity of industrial discharge points in the upstream sector, leading to a higher concentration of dissolved ions. Specifically, these high values are indicative of industrial effluents containing heavy metals – such as Pb, Zn, Hg, As, Cd, and Cu – which significantly increase the electrolytic capacity of the water and sediments (Fitriani et al., 2021).

Electrical conductivity (EC) analysis

According to established environmental quality standards, non-polluted freshwater typically exhibits EC values below 500 µS/cm (Kirana et al., 2026). However, the results from both sdm1 and sdm2 far exceed this recommended threshold. This substantial deviation provides robust evidence that the Cikijing River has undergone severe anthropogenic contamination, as the measured conductivity levels are nearly five times higher than the baseline safety limit.

Table 2. Summary of subsurface interpretation for lines 1, 2, 3, and 4

Survey Line	Lateral distance (m)	Depth (m)	Interpretation
1	0.75–22.75	0–0.5	Topsoil
	0.75–22.75	0.5–4.5	Clay
	1.5–22.0	0.5–4.2	Contaminated clay
	9.5–14.5	1.9–4.9	Dense sandy gravel
2	0.75–22.75	0–0.5	Topsoil
	0.75–22.75	0.5–4.5	Clay
	1.25–22.5	0.5–4.3	Contaminated clay
	9.5–13.0	4.3–4.9	Dense sandy gravel
3	0.75–22.75	0–0.5	Topsoil
	0.75–22.75	0.5–4.3	Clay
	1.25–22.5	0.5–3.3	Contaminated clay
	8.0–15.0	2.0–4.9	Dense sandy gravel
4	0.75–22.75	0–0.5	Topsoil
	0.75–22.75	0.5–4.9	Clay
	1.25–22.0	0.5–3.8	Contaminated clay
	10.0–14.5	2.7–4.9	Dense sandy gravel

Table 3. Physicochemical parameters: pH, EC, and TDS analysis of sediments

Sediment Sample	Replicate	pH	EC (µS/cm)	TDS (ppm)
sdm1	1	5.3	2.78	> 1,999
	2	5.4	2.69	> 1,999
	3	5.5	2.67	> 1,999
	Average	5.4	2.71	> 1,999
sdm2	1	5.7	2.41	> 1,999
	2	6.1	2.75	> 1,999
	3	6.1	2.83	> 1,999
	Average	5.7	2.66	> 1,999

Total dissolved solids (TDS) analysis

The analytical data from Table 3 reveals that TDS concentrations at both sdm1 and sdm2 consistently exceed 1,999 ppm, significantly surpassing the permissible thresholds for clean water. According to the World Health Organization (WHO), the upper limit for non-polluted freshwater is established at 1.000 mg/L (or 1.000 ppm). This substantial elevation in TDS is likely driven by cumulative industrial discharge over time, resulting in a high load of dissolved organic and inorganic matter that significantly degrades water quality (Putri and Afdal, 2023). Referencing the water quality criteria established by Alabaster and Lloyd (2013), the TDS levels in the Cikijing River fall within the "critically poor and hazardous" category, providing definitive evidence of severe contamination.

Synthesis of geophysical and physicochemical correlation

The laboratory analysis of sediment samples conclusively demonstrates that the Cikijing River has undergone severe environmental contamination. This is empirically evidenced by the strong correlation between the anomalously low resistivity values (2.63–9.82 Ωm and the degraded physicochemical parameters (pH, EC, and TDS), all of which fall significantly outside the regulatory safety thresholds for clean water. Notably, the peak concentrations of these pollutants are concentrated in the upstream sector, with a slight attenuation observed in the downstream reach. Despite this minor reduction, the downstream values remain well above the established environmental quality standards, indicating persistent anthropogenic loading.

The high TDS and EC values recorded in the contaminated layers are directly linked to the increased ionic concentration within the riverine system. As the concentration of dissolved ions rises, the electrolytic conductivity of the medium increases, which inversely reduces the bulk resistivity of the subsurface strata. Furthermore, this elevated ionic load – likely associated with heavy metal enrichment – contributes to the acidification of the water, resulting in the observed low pH levels. Therefore, a clear physical relationship is established: resistivity exhibits a direct correlation with pH, while maintaining an inverse relationship with both EC and TDS. This multi-parameter alignment validates the use of electrical resistivity tomography as a robust proxy for mapping industrial contaminant plumes in clay-dominated environments.

CONCLUSIONS

The integrated electrical resistivity and physicochemical analysis provides consistent evidence of shallow subsurface alteration associated with anthropogenic inputs in the Cikijing river area. Subsurface resistivity measurements range from 2.63 Ωm to 375 Ωm, with persistent low-resistivity zones (2.63–9.82 Ωm) identified at depths of approximately 0.5–4.3 m across all survey lines. These anomalies are laterally continuous (approximately 1.0–22.5 m) and confined within a clay-dominated layer, indicating a laterally extensive conductive zone rather than isolated features. Sediment physicochemical analyses support the geophysical observations, with EC values up to 2.710 µS/cm, acidic pH (5.4–5.7), and TDS exceeding 1,999 ppm. These values exceed common environmental thresholds and indicate significant ionic enrichment within the system, rather than directly confirming specific contaminants. The agreement between low-resistivity zones and elevated EC/TDS suggests that pore-fluid conductivity is a dominant control on the geoelectrical response; however, this relationship is interpreted

qualitatively and has not been statistically quantified. The results indicate that the clay layer functions as a key medium for contaminant retention and lateral migration, although this interpretation remains indirect and may also reflect natural controls such as clay content, surface conductivity, and moisture variability. Overall, this study demonstrates that electrical resistivity tomography, integrated with basic physicochemical analysis, provides a reliable first-order approach for delineating subsurface electrical anomalies potentially associated with anthropogenic contamination in alluvial environments, without overstating definitive causation. Importantly, the repeatability of anomaly patterns across multiple profiles highlights the robustness of the integrated approach for preliminary environmental assessment in data-limited settings. However, further validation using direct geochemical tracers is required to fully constrain the origin and composition of the observed anomalies.

Acknowledgements

The authors would like to express their sincere gratitude for the support provided during this research and extend their appreciation to the lecturers, students, and technical staff of the Geophysics Laboratory, as well as to the Geophysics and Physics students from the Faculty of Engineering and the Faculty of Mathematics and Natural Sciences, Universitas Syiah Kuala. The authors also convey their special thanks to the Department of Geophysics, Faculty of Mathematics and Natural Sciences, Universitas Padjadjaran, for their valuable support and collaboration in this research.

REFERENCES

1. Abdel Maleck, M. M., Cheikh Zamel, M. L., Ahmed Elmamy, C. A., Driss, B., Mohamed Abdellahi, M. V. (2024). Physico-chemical and microbiological pollution of industrial wastewater from Levrier Bay in Mauritania. *Journal of Ecological Engineering, 25*(4), 370–379. https://doi.org/10.12911/22998993/185305
2. Adestina, O. B., Paul, E. D., Nuhu, A. A., Onoyima, C. C., Okibe, F. G. (2024). Dynamics of physicochemical parameters as indicators of water quality: A study of Ogun River, Nigeria. *Indonesian Journal of Chemical Analysis, 7*(2), 109–122. https://doi.org/10.20885/ijca.vol7.iss2.art2
3. Ahsan, M. A., Satter, F., Siddique, M. A. B., Akbor, M. A., Ahmed, S., Shajahan, M., Khan, R. (2019). Chemical and physicochemical characterization of effluents from the tanning and textile industries using a multivariate statistical approach. *Environmental Monitoring and Assessment, 191*(9), 575. https://doi.org/10.1007/s10661-019-7654-2
4. Alabaster, J.S. and Lloyd, R.S. (2013) *Water Quality Criteria for Freshwater Fish* (No. 3117). Elsevier, Amsterdam.
5. Alao, J. O., Lawal, K. M., Dewu, B. B. M., Raimi, J. (2024). Detection of shallow underground targets using electrical resistivity tomography and the implications in civil/environmental engineering. *Discover Geoscience, 2*(1), 52. https://doi.org/10.1007/s44288-024-00058-6
6. Angi, J. C. W., Al Mukarramah, N. H., Maskun, M. (2025). Mitigating water depletion through wastewater management law in Indonesia's textile sector: Evaluating compliance and alignment with national environmental standards. *BIO Web of Conferences*, *155*, 06017. https://doi.org/10.1051/bioconf/202515506017
7. Appiah, I., Wemegah, D. D., Asare, V. D. S., Danuor, S. K., Forson, E. D. (2018). Integrated geophysical characterization of Sunyani municipal solid waste disposal site using magnetic gradiometry, magnetic susceptibility survey and electrical resistivity tomography. *Journal of Applied Geophysics, 153*, 143–153. https://doi.org/10.1016/j.jappgeo.2018.02.007
8. Ashel, H., Taufik, A., Pratomo, P. M., Mawaddah, S., Srigutomo, W. (2021). Application of electrical resistivity method to analyze liquid waste pollution in Linggar Village, Rancaekek, West Java, Indonesia. *AIP Conference Proceedings*, 2320(1), 040013. https://doi.org/10.1063/5.0037596
9. Bernardo, B., Candeias, C., Rocha, F. (2022). Application of geophysics in geo-environmental diagnosis on the surroundings of the Hulene-B waste dump, Maputo, Mozambique. *Journal of African Earth Sciences, 185*, 104415. https://doi.org/10.1016/j.jafrearsci.2021.104415
10. Boonsakul, P., Buddhawong, S., Wangyao, K. (2023). Maximizing RDF recovery potential through the integration of electrical resistivity tomography and frequency-domain electromagnetic surveys for waste characterization in open dump mining. *Science of the Total Environment, 904*, 166807. https://doi.org/10.1016/j.scitotenv.2023.166807
11. De Borba, W.F., Da Silva, J.L.S., da Cunha Kemerich, P.D., Fries, M., Fernandes, G.D., De Souza, É.E., Ilha, L.M. and Da Silva, G.S.N. (2023). Assessment of an urban waste disposal contamination using chemical analysis and DC resistivity. *International Journal of Environmental Science*

and Technology, 20(7), 7939-7950. https://doi.org/10.1007/s13762-022-04496-y

12. Delinom, R. M. (2009). Structural geology controls on groundwater flow: Lembang fault case study, West Java, Indonesia. *Hydrogeology Journal, 17*(4), 1011–1023. https://doi.org/10.1007/s10040-009-0453-z
13. Dewi, N. A., Tohari, A., Muttaqien, I. (2020). Evaluation of liquefaction potential in the Bandung Basin based on the multi-sensor surface wave analysis method (In Bahasa Indonesia). *Riset Geologi dan Pertambangan, 30*(2), 241–256. https://jrisetgeotam.brin.go.id/index.php/jrisgeotam/article/view/1131
14. Eze, S. U., Abolarin, M. O., Ozegin, K. O., Bello, M. A., William, S. J. (2022). Numerical modeling of 2-D and 3-D geoelectrical resistivity data for engineering site investigation and groundwater flow direction study in a sedimentary terrain. *Modeling Earth Systems and Environment, 8*(3), 3737–3755. https://doi.org/10.1007/s40808-021-01325-y
15. Fitriani, D., Utami, W., Kirana, K. H., Agustine, E., Zulaikah, S. (2021). Magnetic signatures on river sediments and agricultural soils as proxy indicators of anthropogenic-derived pollution (Case study: Cikijing River, Rancaekek, West Java). *Jurnal Penelitian Pendidikan IPA, 7*(3), 381–387. https://doi.org/10.29303/jppipa.v7i3.697
16. Geetha T. S., Gandhimathi, G., Chellaswamy, C., Thiruvalar Selvan, P. (2024). Comprehensive river water quality monitoring using convolutional neural networks and gated recurrent units: A case study along the Vaigai River. *Journal of Environmental Management, 365*, 121567. https://doi.org/10.1016/j.jenvman.2024.121567
17. Ibuot, J. C., Aka, M. U., Inyang, N. J., Agbasi, O. E. (2024). Georesistivity and physicochemical evaluation of hydrogeologic units in parts of Akwa Ibom State, Nigeria. *International Journal of Energy and Water Resources, 8*(1), 111–122. https://doi.org/10.1007/s42108-022-00191-3
18. Ibuot, J. C., Okeke, F. N., George, N. J., Obiora, D. N. (2017). Geophysical and physicochemical characterization of organic waste contamination of hydrolithofacies in the coastal dumpsite of Akwa Ibom State, Southern Nigeria. *Water Science and Technology: Water Supply, 17*(6), 1626–1637. https://doi.org/10.2166/ws.2017.066
19. Kanan, A. H., Marine, S. S., Raihan, F., Redowan, M., Miah, M. (2014). Textile effluents change physicochemical parameters of water and soil: Threats to agriculture. *African Journal of Agronomy, 2*(10), 219–223. https://internationalscholarsjournals.org/articles/5702543603112014
20. Kementerian Kesehatan Republik Indonesia. (2023). *Minister of Health Regulation Number 2 of 2023 concerning the implementation of Government Regulation Number 66 of 2014 on environmental health* (In Bahasa Indonesia). https://peraturan.bpk.go.id/Details/245563/permen
21. Kementerian Lingkungan Hidup dan Kehutanan Republik Indonesia. (2023). *Daily water quality status (Status mutu air harian)* (In Bahasa Indonesia). https://ppkl.menlhk.go.id/onlimo-2022/
22. Kirana, K.H., Iman, M.R.R., Shafaria, M., Agustine, E., Fitriani, D., Subehi, L., Rusydi, A.F., Yustiawati and Tamuntuan, G.H. (2026). Physicochemical characteristics and potentially toxic elements in sediments of the midstream of Citarum river around hydroelectric power plants. *Soil and Sediment Contamination: An International Journal, 35*(1), 109–128. https://doi.org/10.1080/15320383.2025.2519758
23. Kondracka, M., Stan-Kłeczek, I., Sitek, S., Ignatiuk, D. (2021). Evaluation of geophysical methods for characterizing industrial and municipal waste dumps. *Waste Management, 125*, 27–39. https://doi.org/10.1016/j.wasman.2021.02.015
24. Loke, M. H. (2004). *Tutorial: 2-D and 3-D electrical imaging surveys*. www.geotomosoft.com
25. Lowrie, W., Fichtner, A. (2020). *Fundamentals of geophysics*. Cambridge University Press.
26. Marselina, M., Wijaya, M. (2024). Heavy metals in water and sediment of Cikijing River, Rancaekek District, West Java: Contamination distribution and ecological risk assessment. *PLOS ONE, 19*(4), e0294642. https://doi.org/10.1371/journal.pone.0294642
27. Maryudhaningrum, S. T., Cakrabuana, W., Marthakusuma, L., Sarah, D., Sadisun, I. A., Pamumpuni, A., Soebowo, E. (2025). Land subsidence due to groundwater extraction and natural consolidation in the Bandung Basin, West Java, Indonesia. *Riset Geologi dan Pertambangan 35*(1), 25–36. http://dx.doi.org/10.55981/risetgeotam.2025.1363
28. Miswar, H., Wahyuni, A. (2017). Identification of liquid waste seepage using the geoelectrical resistivity method in the Makassar Industrial Area (KIMA) (In Bahasa Indonesia). *JFT: Jurnal Fisika dan Terapannya, 4*(2), 215–224. https://doi.org/10.24252/jft.v4i2.10257
29. Musawwa, M. M., Sarkawi, M., Arrunillah, D., Sazawa, K., Mohan, G., Kuramitz, H. (2026). Review of traditional batik wastewater treatment in Indonesia to address environmental and health hazards and support sustainable practices of micro, small, and medium enterprises. *Discover Environment, 4*(1), 18. https://doi.org/10.1007/s44274-025-00466-6
30. Novaliana, R. N., Herawati, H., Sahidin, A., Arief, M. C. (2025). Distribution of chromium in water and sediment in the Cibaligo River, Cimahi City, West Java Province. *Aquaculture, Aquarium, Conservation & Legislation, 18*(5), 2100–2113. https://bioflux.com.ro/docs/2025.2100-2113.pdf

31. Nugroho, S. A., Wilopo, W., Lathif, I. F. A., Taufiq, A. (2025). Seawater Intrusion Assessment based on Geological, Hydrogeological, Cl/Br vs Cl Graphical Analysis, Recharge Area, and Groundwater Usage in Makassar Coastal Area, South Sulawesi, Indonesia. *Journal of Applied Geology, 9*(2), 109. http://dx.doi.org/10.22146/jag.101429
32. Prananda, Y., Taufik, F., R, A., S, F., T, M. H., Widodo. (2017). Pollution detection of hazardous and toxic substance disposal using magnetic susceptibility method in Cikijing River, Rancaekek. *AIP Conference Proceedings, 1861*(1), 030039. https://doi.org/10.1063/1.4990926
33. Putri, D. A., Afdal, A. (2023). Water pollution profile of the Cikijing River in Bandung and Sumedang Regencies (In Bahasa Indonesia). *Jurnal Fisika Unand, 12*(4), 541–547. https://doi.org/10.25077/jfu.12.4.541-547.2023
34. Reynolds, J. M. (2011). *An introduction to applied and environmental geophysics*. John Wiley & Sons.
35. Rifai, M., Harintaka. (2025). Analysis of water quality dynamics of Sentarum Lake, Indonesia, with water index application and water parameter algorithm methods using Google Earth Engine. *IOP Conference Series: Earth and Environmental Science, 1443*(1), 012012. https://doi.org/10.1088/1755-1315/1443/1/012012
36. Sabrian, P. G., Saepuloh, A., Septyandy, M. R., Heriyanto, Putri, A. D. (2024, July). Detection and mechanical interpretation of surface displacement by volcanic and anthropogenic interactions around Bandung Basin, through multi temporal interferometric SAR (MT-InSAR) technique. *IOP Conference Series: Earth and Environmental Science, 1378*(1), 012007. https://doi.org/10.1088/1755-1315/1378/1/012007
37. Saputra, H., Fadhli, Z., Safitri, R., Syukri, M. (2024). Integrated geophysical analysis for landslide risk mitigation: a case study on the weak zone area of Jantho-Lamno Route, Aceh, Indonesia. *International Journal of GEOMATE, 26*(113), 41–49. https://doi.org/10.21660/2024.113.4184
38. Satriyo, N. A., Mulyono, A., Wibawa, S., Yuliyanti, A., Sari, A. M., Putra, Moch. H. Z., Arfiyansyah, K. (2025). The review of the geological disaster of Bandung Basin subsurface: perspective from geological approach. *Geology, Ecology, and Landscapes, 9*(3), 933–951. https://doi.org/10.1080/24749508.2024.2359781
39. Silitonga, P.H., 1973. Peta Geologi Lembar Bandung, Jawa, skala 1:100.000. Direktorat Geologi, Bandung. https://search.worldcat.org/title/Peta-geologi-lembar-Bandung-Djawa-Geologic-map-of-the-Bandung-quadrangle-Java-by-P.H.-Silitonga/oclc/21685344
40. Syukri, M., Fadhli, Z., Hasibuan, P., Saputra, H., Safitri, R. (2025b). Recent developments in the use of geoelectric surveys for in investigating causes of road pavement failure: A case study along Darussalam road, Aceh, Indonesia. *Ecological Engineering & Environmental Technology (EEET), 26*(10), 128–139. https://doi.org/10.12912/27197050/210524
41. Syukri, M., Fadhli, Z., Saputra, H., Safitri, R. (2025a). Geophysical assessment of liquefaction hazards and environmental implications in Pidie Jaya, Indonesia. *Ecological Engineering & Environmental Technology, 26*(11), 204-216. https://doi.org/10.12912/27197050/211865
42. Syukri, M., Saad, R., Abubakar, M. (2013). Leachate migration delineation using 2-D electrical resistivity imaging (2-DERI) at Gampong Jawa, Banda Aceh. *Electronic Journal of Geotechnical Engineering, 18*, 1505–1510.
43. Syukri, M., Saad, R., Fadhli, Z. (2020). Capability of P- and S-wave seismic refraction in delineating the Blang Bintang sanitary landfill subsurface. *Songklanakarin Journal of Science and Technology, 42*, 780–787. https://sjst.psu.ac.th/article/2213
44. Telford, W.M., Geldart, L.P., Sheriff, R.E., Keys, D.A., (1990). *Applied Geophysics*. Cambridge University. USA.
45. Tirtomihardjo, H. (2016). Groundwater environment in Bandung, Indonesia. *In Groundwater environment in Asian cities* (pp. 193–228). Butterworth-Heinemann. https://doi.org/10.1016/B978-0-12-803166-7.00010-6
46. Wangsaatmaja, S., Sutadian, A. D., Prasetiati, M. A. (2006). A review of groundwater issues in the Bandung Basin, Indonesia: Management and recommendations. *Int Rev Environ Strateg, 6*(2), 425–441. https://www.iges.or.jp/en/pub/review-groundwater-issues-bandung-basin/en
47. Zhou, Q., Le, Q. V., Meng, L., Yang, H., Gu, H., Yang, Y., Peng, W. (2022). Environmental perspectives of textile waste, environmental pollution and recycling. *Environmental Technology Reviews, 11*(1), 62–71. https://doi.org/10.1080/21622515.2021.2017000